Available online at www.sciencedirect.com
SCIENCE DIRECT®
Journal of Power Sources 125 (2004) 299–308
JOURNAL OF POWER SOURCES
www.elsevier.com/locate/jpowsour

Effects of electrolytes and electrochemical pretreatments on the capacitive characteristics of activated carbon fabrics for supercapacitors

Chi-Chang Hu*, Chen-Ching Wang

Department of Chemical Engineering, National Chung Cheng University, Chia Yi 621, Taiwan

Received 4 February 2003; received in revised form 30 July 2003; accepted 6 August 2003

Abstract

The capacitive characteristics of activated carbon fabrics (ACFs) coated on the graphite substrates were systematically investigated by means of cyclic voltammetry and the galvanostatic charge–discharge technique. Effects of the PVDF contents in the electronically conductive binder, electrochemical pretreatments, and the electrolytes on the capacitive performance of ACFs were compared in aqueous media. These ACF-pasted electrodes showed the more ideally capacitive responses in 1 M $NaNO_3$ with a specific capacitance of 76 F g^{-1} when the electronically conductive binder contained 40 wt.% PVDF. The specific capacitance of ACF-pasted electrodes reached a maximum in 0.5 M H_2SO_4 (about 153 F g^{-1} measured at 25 mV s^{-1}), due to the presence of a suitable density of oxygen-containing functional groups, when they were subjected to the *potentiostatic polarization* at 1.8 V (versus reversible hydrogen electrode (RHE)) or *potentio-dynamic polarization* between 1.3 and 1.8 V in $NaNO_3$ for 20 min. The oxygen-containing functional groups within the electrochemically pretreated ACFs were identified by means of X-ray photoelectron spectroscopy (XPS).

Keywords: Activated carbon fabric; PVDF; Electrochemical pretreatment; Electrolyte; Supercapacitors

1. Introduction

Due to the unique characteristics of a much higher energy density and a much higher power density (PD) in comparing with conventional capacitors and batteries, respectively, the development of supercapacitors for power sources delivering significant energy in the high-power or pulse-power forms has become the interesting subjects of many researches [1–3]. The relatively high energy density of supercapacitors relied on either the low-density materials with high specific surface areas providing for the electrical double-layer capacitance [1,2,4–6] or the electroactive materials with high Faradaic pseudocapacitance [3,7–9]. The former devices are usually called double-layer capacitors meanwhile the latter devices are also called pseudocapacitors or captteries since the mechanism of energy storage within the electroactive materials is very similar to that of rechargeable batteries [1].

Carbon materials, including activated carbon powders, carbon fabrics, and carbon nanotubes (CNT) [1,2,4–6,10–12], are widely studied for the application of double-layer capacitors since these materials in several forms are usually of high surface areas. Moreover, candidates with good capacitive characteristics, formed from cheaper precursors, have attracted much attention due to the cost consideration. Since the electrochemical properties of carbon materials can be modified by thermal or laser activation [13,14], etching [4,15], electrochemical pretreatments [16,17], polishing [18], etc., carbon with various pretreatments is believed to exhibit significant pseudocapacitance mainly coming from the oxygen functional groups. These oxygen-containing functional groups providing the active centers for specific adsorption and/or ion exchange as well as the Faradaic redox transitions [19,20] should enhance the specific capacitance of modified carbon materials. In addition, these oxygen-containing functional groups can be easily formed by means of potentiostatic or potentiodynamic techniques in aqueous media [16,17,20]. Based on the above opinions, activated carbon fabrics (ACFs) with electrochemical treatments are considered as a potential candidate for the electrode materials applicable in supercapacitors.

In this work, effects of "mild" electrochemical pretreatments (i.e., $E < 2.0$ V versus reversible hydrogen electrode (RHE)) in aqueous electrolytes on the capacitive behavior of ACF-pasted graphite electrodes were systematically inves-

* Corresponding author. Tel.: +886-5-2720411x33411; fax: +886-5-2721206.
E-mail address: chmhcc@ccu.edu.tw (C.-C. Hu).

0378-7753/$ – see front matter © 2003 Elsevier B.V. All rights reserved.
doi:10.1016/j.jpowsour.2003.08.002

tigated by voltammetric and galvanostatic charge–discharge techniques. In addition, effects of the PVDF (an insulated binder) content in the electronically conductive binding paste on the electrochemical properties of ACF-pasted electrodes are also compared. The chemical states and amounts of oxygen-containing function groups on ACFs were characterized by X-ray photoelectron spectroscopy (XPS).

2. Experimental

Polyacrylonitrile (PAN)-derived activated carbon fabrics (ACFs) were served as the basic electrode materials for the electrochemical investigations of electrical double-layer capacitors (EDLC). The mean thickness of these fabrics is ca. 0.48 mm, which were bound onto 10 mm × 10 mm × 3 mm graphite substrates with a graphite-powder paste. These substrates before binding with ACFs were first abraded with ultrafine SiC paper, degreased with acetone and water, then etched in a 0.1 M HCl solution at room temperature (ca. 26 °C) for 10 min, and finally degreased with water in an ultrasonic bath. The exposed geometric area of these pretreated graphite supports is equal to 1 cm^2 while the other surface areas were insulated with polytetrafluorene ethylene (PTFE) coatings. The graphite paste slurries ground for 30 min were composed of fine graphite powders with a low specific surface area (2.8 $m^2\,g^{-1}$), PVDF powders, and *N*-methyl-2-pyrrolidone in variable ratios. The bubbles within the slurries were removed ultrasonically for 10 min before usage. The total amount of the binding paste on each electrode was kept approximately constant (ca. 0.03 $g\,cm^{-2}$) to avoid any unexpected influences. These electrodes were dried in a vacuum oven at 85 °C overnight.

The weight of each ACF was measured through a microbalance with an accuracy of 10 μg (Sartorius BP 211D, Germany). The specific surface area and pore volume of ACFs were determined with an automated adsorption apparatus (Micromeritics, ASAP 2020) with liquid nitrogen adsorption at −196 °C. The specific surface area and micropore volumes of ACFs were calculated on the basis of Brunauer–Emmett–Teller (BET) and Dubinin–Radushkevich (D–R) equations, respectively. X-ray photoelectron spectroscopic measurements were performed with an ESCA 210 (VG Scientific Ltd.) spectrometer. XPS spectra employed Mg Kα ($h\nu = 1253.6$ eV) irradiation as the photosource, with a primary voltage of 12 kV and an emission current 17 mA. The analysis chamber pressure during scans was approximately 10^{-10} mbar.

Electrochemical measurements for all ACFs with and without electrochemical pretreatments were performed by means of an electrochemical analyzer system, CHI 633A (CH Instruments, USA). All experiments were carried out in a three-compartment cell. An Ag/AgCl electrode (Argenthal, 3 M KCl, 0.207 V versus SHE at 25 °C) was used as the reference and a piece of platinum gauze with an exposed area equal to 4 cm^2 was employed as the counter electrode. A Luggin capillary, whose tip was set at a distance of 1–2 mm from the surface of the working electrode, was used to minimize errors due to *i*R drop in the electrolyte. The potentiodynamic polarization of an ACF-pasted electrode was performed by means of cyclic voltammetry between 1.3 and 1.8 V (versus reversible hydrogen electrode (RHE) at 25 $mV\,s^{-1}$ for 20 min. The potentiostatic polarization was anodically polarized at 1.8 V (versus RHE) for 20 min.

All solutions used in this work were prepared with 18 MΩ cm water produced by a reagent water system (MILLI-Q SP, Japan), and all reagents not otherwise specified in this work were Merck, GR. In addition, the electrolytes used to study the capacitive behavior of ACFs were degassed with purified nitrogen gas before measurements, and nitrogen was passed over the solutions during the measurements. The solution temperature was maintained at 25 °C by means of a water thermostat (HAAKE DC3 and K20).

3. Results and discussion

3.1. Effects of the PVDF content on the capacitive characteristics of ACFs

Typical voltammetric behavior of an ACF without and with a graphite current collector (i.e., the ACF-pasted electrode) measured in 1 M $NaNO_3$ at 25 $mV\,s^{-1}$ is shown in Fig. 1 as curves 1 and 2, respectively. From a comparison of curves 1 and 2, two features have to be considered. First, the maximum currents on both positive and negative sweeps of curve 2 are lower than that of curve 1, probably due to the fact that partial pores of ACF on the current collector side were closed with the graphite paste. On the other hand, the total voltammetric charges surrounded within curve 1 is much lower than that within curve 2, indicating a higher capacity of an ACF-pasted electrode. Second, a rise in currents with the positive shift of electrode potentials on both

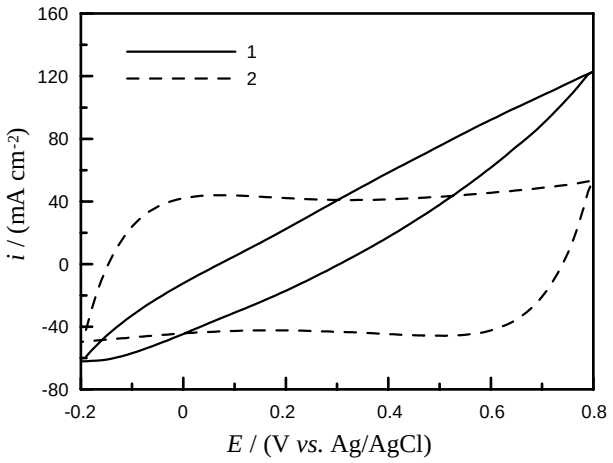

Fig. 1. CV curves in 1 M $NaNO_3$ at 25 $mV\,s^{-1}$ for ACF electrodes (1) without and (2) with a graphite current collector bound with the graphite-PVDF (40 wt.%) paste.

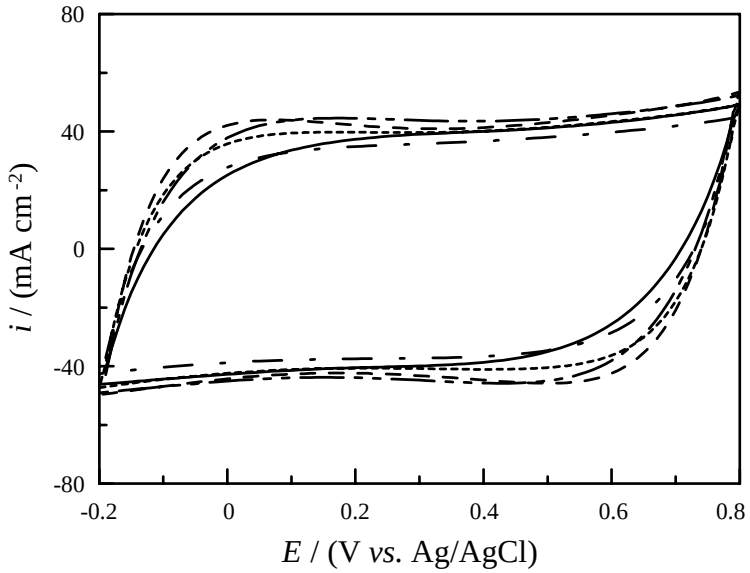

Fig. 2. CV curves of ACF-pasted electrodes measured in 1 M $NaNO_3$ at 25 mV s^{-1}. The amount of PVDF in the electronically conductive paste is: 1 (—) 10 wt.%; 2 (— - —) 20 wt.%; 3 (- - - -) 30 wt.%; 4 (– – –) 40 wt.%; and 5 (— -- —) 60 wt.%.

positive and negative sweeps in the whole potential range of investigation is clearly observed on curve 1, indicating that the electric resistance of ACF is significant. In fact, at a much slower scan rate (i.e., 1 mV s^{-1}, not shown here), a more rectangular-like *i–E* curve is obtained on this ACF without the current corrector, indicating that ACF cannot be used along in the application of supercapacitors. Therefore, in order to reach the pulse-power demand of a supercapacitor mainly composed of ACF, the employment of a current collector is necessary.

Typical voltammetric responses in $NaNO_3$ for various ACF-pasted electrodes with the PVDF contents of 10, 20, 30, 40, and 60 wt.% in the binding paste are shown in Fig. 2 as curves 1–5, respectively. Note that a more rectangular-like *i–E* curve is obtained with increasing the PVDF content in the paste when the PVDF content is less than or equal to 40 wt.% while an opposite result is obtained as the PVDF contents above 40 wt.%. The former result indicates that the electrical contact resistance between ACF and the graphite current collector can be reduced with increasing the binder content in the paste. This is reasonable due to the better connection between graphite powders in the paste, favoring the electron hopping between the graphite powders. On the other hand, due to the insulated characteristics of PVDF, the surface of graphite powders in the paste should be coated with large amount of PVDF, resulting in the closure of electron paths between the graphite powders. Hence, an optimal content of PVDF, 40 wt.%, in the paste is obtained.

3.2. Effects of electrolytes on the capacitive characteristics of ACFs

The *i–E* curves of an ACF-pasted electrode measured in 1 M $NaNO_3$, 0.5 M H_2SO_4, and 0.5 M Na_2SO_4 at 25 mV s^{-1} are shown in Fig. 3 as curves 1–3, respectively. On curve 1, very high background currents are clearly found on both positive and negative sweeps in the whole potential range of investigation (i.e., from −0.2 to 0.8 V). This capacitive-like and symmetric *i–E* response indicates that ACF-pasted graphite electrodes exhibits the electrochemical characteristics suitable for the application of supercapacitors in 0.5 M $NaNO_3$. Moreover, the voltammetric charges on the positive and negative sweeps are approximately equal, indicating the ideal reversibility of the double-layer charging–discharging characteristics of this ACF-pasted electrode, further supporting its promising potential in the supercapacitor application. On curve 2, larger background currents but less symmetric *i–E* responses are clearly found since a slight rise in currents with the positive shift of electrode potentials on both positive and negative sweeps in the whole potential range of investigation is observed for this electrode. The above difference indicates that the capacitive performance of ACF in $NaNO_3$ is better than that in H_2SO_4 although the total charge stored in the latter case is larger than that in the former case. On curve 3, the voltammetric behavior of this ACF-pasted electrode is similar in shape to that of curve 1 while lower voltammetric currents on both positive and negative sweeps are clearly observed on curve 3, especially in the more positive potential region. A comparison of curves 1–3 reveals the fact that the double-layer capacitance of ACF is a strong function of the electrolyte employed. The lower specific capacitance of curve 3 in comparison with curve 1 should be due to the larger ionic solvation radius of SO_4^{2-} because of its higher charge density and the larger atom number in comparison with NO_3^-. On the other hand, due to the proton hopping mechanism in aqueous media [21], the specific capacitance measured in the acidic solution is reasonably larger than that measured in nearly neutral media.

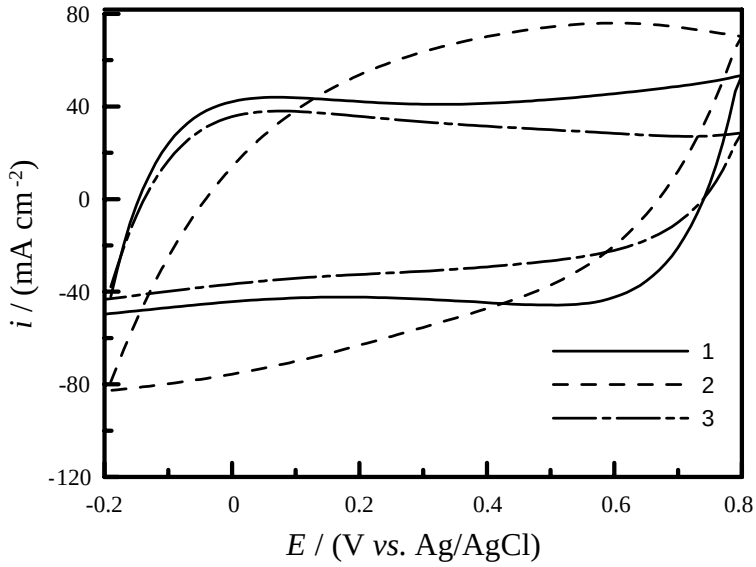

Fig. 3. CV curves in (1) 1 M $NaNO_3$; (2) 0.5 M H_2SO_4; and (3) 0.5 M Na_2SO_4 at 25 mV s^{-1} for an ACF-pasted electrode (40 wt.% of PVDF in the paste).

The voltammetric responses of an ACF-pasted electrode measured in 0.5 M $NaNO_3$ at different scan rates of CV are shown in Fig. 4a. In addition, the dependence of voltammetric currents on the scan rate of CV for this ACF-pasted electrode is shown in Fig. 4b. Note in Fig. 4a that all CV curves show the typical capacitive-like characteristics. In addition, there exists approximately linear dependence of voltammetric currents on the scan rate of CV in Fig. 4b. These results indicate that the charge–discharge responses of the electric double-layer are highly reversible. Hence, ACF-pasted electrodes show the high-power property, meeting one of the basic requirements for the electrode materials of supercapacitors. On the other hand, the potential windows for current-rising and -decaying to the plateau values become wider with increasing the scan rate of CV when the direction of potential sweeps is just changed (see Fig. 4a). The above behavior shows a less reversible character of this electrode under a faster scan rate. This phenomenon should result from the fact that most pores within this ACF are microporous (see further). Note that the charge–discharge current of the electric double layer is directly proportional to the scan rate of CV meanwhile the diffusion barrier of solvated ions within the pores distributed within the ACF should be increased with decreasing the pore size. Thus, the *i*R drop due to the electrolyte resistance within these micropores is expected to become significant at a higher scan rate, resulting in a less reversible behavior under a higher scan rate of CV.

Curves 1–3 in Fig. 5 shows the dependence of specific capacitance for an ACF-pasted electrode on the scan rate of CV in 1 M $NaNO_3$, 0.5 M H_2SO_4, and 0.5 M Na_2SO_4. Note that an obvious decrease in specific capacitance of this ACF-pasted electrode with increasing the scan rate of CV is clearly found on curve 2 while this phenomenon is not found for curves 1 and 3. The above result indicates that the specific capacitance of ACF in H_2SO_4 is significantly decreased with increasing the scan rate of CV. This is reasonably attributed to the microporous nature of ACF since the rate of ion rearrangement in the electric double layer is not as fast as the rate of potential change (i.e., scan rates of CV). This is especially true for the inner surface areas of micropores, not freely accessible for solvated ions. Thus, these inner surface areas do not completely provide the double-layer capacitance at higher scan rates of CV, resulting in the significant decrease in specific capacitance of the ACF-pasted electrode. On the other hand, from a comparison of curves 1–3 in Fig. 5, the electrolyte with respect to decreasing the specific capacitance of ACF is: $H_2SO_4 > NaNO_3 > Na_2SO_4$ at all scan rates, which has been found in Fig. 2. Accordingly, certain inner areas partially accessible by protons should not provide double-layer capacitance when $NaNO_3$ and Na_2SO_4 are employed. Based on the above results and discussion, the total available specific capacitance and the portion of inaccessible surface areas within the ACF-pasted electrode are strongly dependent on the electrolytes employed.

The above ACF-pasted electrode was subjected to the galvanostatic charge–discharge examination to evaluate its capacitive behavior. Typical chronopotentiograms measured in 1 M $NaNO_3$ between −0.2 and 0.8 V at 10, 20, and 30 mA cm^{-2} are shown in Fig. 6 as curves 1–3, respectively. The average specific capacitance of this ACF-pasted electrode measured at different current densities can be calculated on the basis of Eq. (1) [1–3,7–9]:

$$C_S = \frac{C}{w} = \frac{i}{[|(dE/dt)| \times w]} \approx \frac{i}{[(\Delta E/\Delta t) \times w]} \quad (1)$$

where C_S, C, w, i, and (dE/dt) indicates the specific capacitance, average capacitance, weight of ACF, current density of charge–discharge, and slope of these charge–discharge curves at a specific time. In this work, the slopes of charge–discharge curves at a specific time are very close

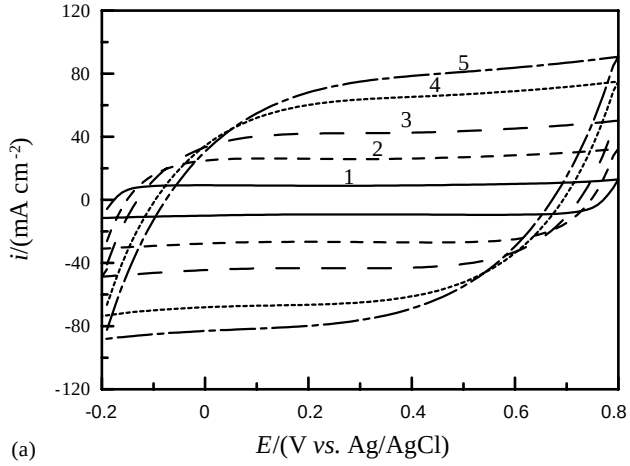

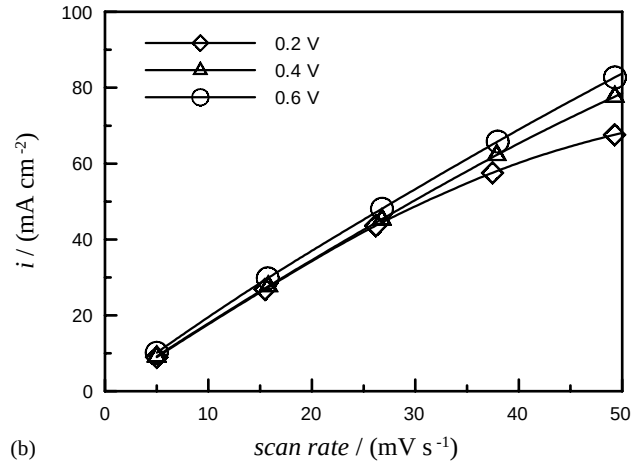

Fig. 4. (a) CV curves in 1 M $NaNO_3$ at (1) 5 mV s^{-1}; (2) 15 mV s^{-1}; (3) 25 mV s^{-1}; (4) 40 mV s^{-1}; and (5) 50 mV s^{-1}; and (b) dependence of voltammetric currents at: (◇) 0.2 V; (△) 0.4 V; and (○) 0.6 V of the negative sweeps on the scan rate of CV for a freshly prepared ACF-pasted electrode (40 wt.% of PVDF in the paste).

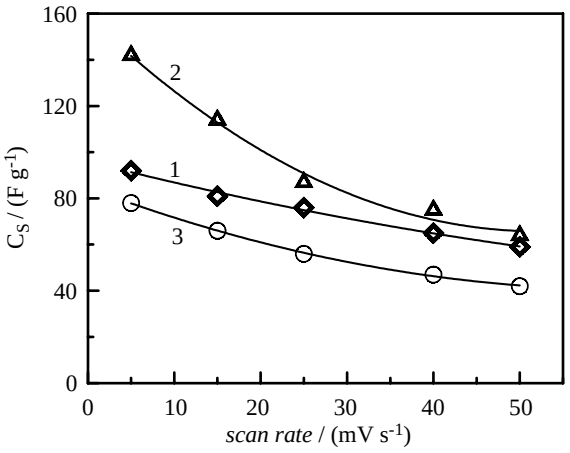

Fig. 5. Dependence of specific capacitance of ACF-pasted electrodes on the scan rate of CV in (1) 1 M $NaNO_3$; (2) 0.5 M H_2SO_4; and (3) 0.5 M Na_2SO_4.

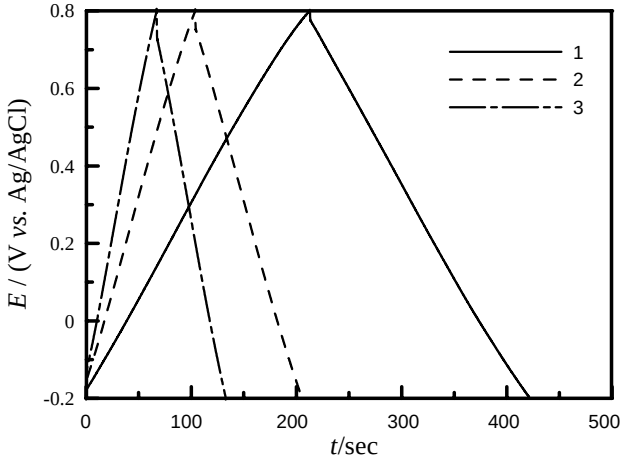

Fig. 6. Chronopotentiograms of an ACF-pasted electrode measured in 1 M $NaNO_3$ between −0.2 and 0.8 V at (1) 10 mA cm^{-2}; (2) 20 mA cm^{-2}; and (3) 30 mA cm^{-2}.

to their mean values since all charge curves are linear and symmetric to their corresponding discharge curves. The specific capacitance of this ACF-pasted electrode measured at 10, 20, and 30 mA cm^{-2} is equal to ca. 91, 88, and 82 F g^{-1}, respectively. Since the specific capacitance measured from the charge–discharge method is only weakly dependent on the applied current density and since all *E*–*t* curves are symmetric, this ACF-pasted electrode in $NaNO_3$ shows the high-power characteristics for the application of supercapacitors. The average power density of the ACF measured at different current densities can be calculated on the basis of Eq. (2):

$$\mathrm{PD} = \frac{C\Delta V^2}{2\,wt} = \frac{i \times \Delta V}{2\,w} \tag{2}$$

where t and ΔV are indicative of the discharge time and potential region of discharge, respectively. The average power density of the ACF measured at 10, 20, and 30 mA cm^{-2} is equal to ca. 0.21, 0.43, and 0.62 kW kg^{-1}, respectively. These results show an acceptable power property of this ACF-pasted electrode, suitable for the application of supercapacitors.

3.3. Effects of electrochemical pretreatments on the capacitive characteristics of ACFs

The specific capacitance of carbon materials should be promoted by the introduction of oxygen functional groups that usually come from pretreatments in aqueous media. These oxygen-containing functional groups may act as the active centers for specific adsorption and/or ion exchange as well as the Faradaic redox transitions [19,20], resulting in the increase in the specific capacitance of modified carbon materials. Since the electrochemical properties of carbon materials can be easily modified by electrochemical methods [16,17], ACFs with electrochemical pretreatments may act as a promising material applicable in supercapacitors.

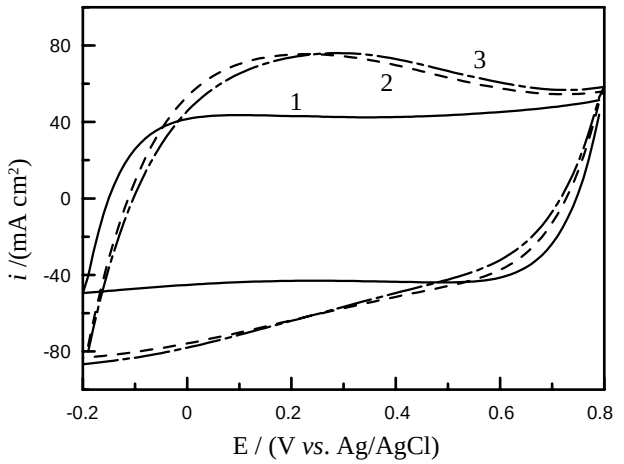

Fig. 7. CV curves of ACF-pasted electrodes with (1) no pretreatment; (2) CV between 1.3 and 1.8 V; and (3) potentiostatic polarization at 1.8 V (vs. RHE) for 20 min in 1 M $NaNO_3$. Voltammetric curves were measured in 1 M $NaNO_3$ at 25 mV s^{-1}.

Typical voltammetric results measured in 1 M $NaNO_3$ for an as-prepared ACF-pasted electrode, an ACF-pasted electrode pretreated with *potentiodynamic polarization* between 1.3 and 1.8 V (versus RHE), and an ACF-pasted electrode modified with *potentiostatic polarization* at 1.8 V (versus RHE) for 20 min in the same medium are shown in Fig. 7 as curves 1–3, respectively. Since curve 1 is very similar in shape to curve 2 in Fig. 1, there is no obvious difference between the as-prepared samples. From a comparison of curves 1 and 2, voltammetric currents on both positive and negative sweeps are significantly increased with the *potentiodynamic polarization* in the mild positive potential region in $NaNO_3$. This increase in capacitive currents should be not due to the increase in surface area of ACF since the increase in voltammetric currents mainly occurs in the low potential region (i.e., $E <$ ca. 0.5 V). Therefore, this effect is more reasonably attributed to the presence of oxygen-containing functional groups through means of electrochemical modification in aqueous media. This modification indeed promotes the specific capacitance of ACF and its electrochemical reversibility is still good although the voltammetric responses loss the typical capacitive behavior (i.e., rectangular shape). Hence, this modified ACF still has potential in the application of supercapacitors. From a comparison of curves 2 and 3, there is no obvious difference in voltammetric behavior between these two modified ACF-pasted electrodes although their modification modes are different. Accordingly, both electrochemical modes are powerful methods for ACF modification. On the other hand, the following samples were only modified by the *potentiostatic polarization* method since the modification by means of direct-current (dc) mode is considered to be more practically useful.

Curves 1 and 2 in Fig. 8a shows a comparison of the voltammetric behavior for an ACF-pasted electrode before and after *potentiostatic polarization* in 0.5 M H_2SO_4 at

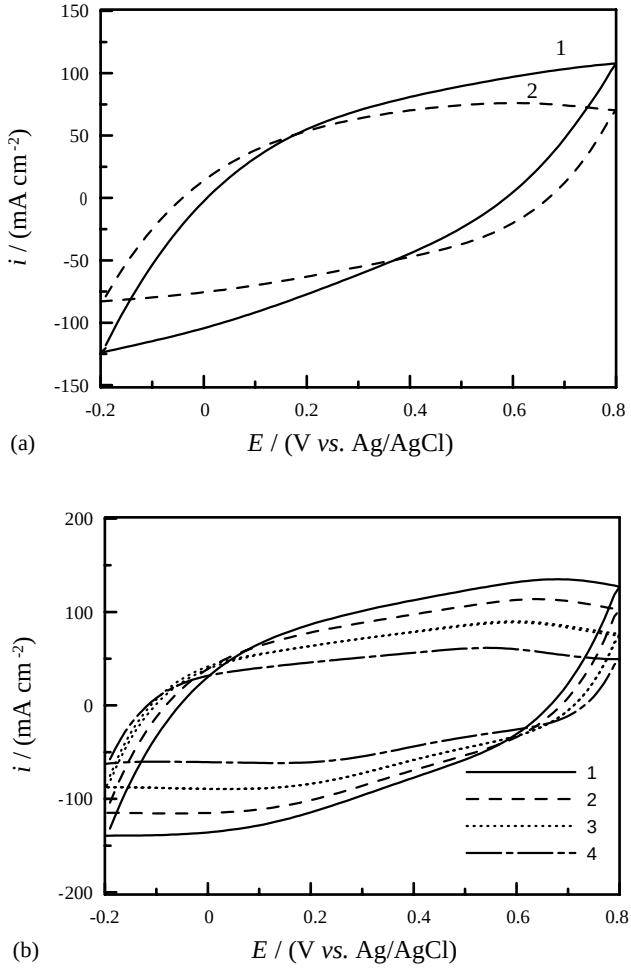

Fig. 8. (a) Voltammetric behavior measured in 0.5 M H_2SO_4 for an ACF-pasted electrode (1) before and (2) after potentiostatic polarization at 1.8 V (vs. RHE) for 20 min in 0.5 M H_2SO_4 and (b) voltammetric behavior measured in 0.5 M H_2SO_4 at (1) 25 mV s^{-1}; (2) 20 mV s^{-1}; (3) 15 mV s^{-1}; and (4) 10 mV s^{-1} for an ACF-pasted electrode with potentiostatic polarization at 1.8 V (vs. RHE) for 20 min in 1 M $NaNO_3$.

1.8 V (versus RHE) for 20 min while the results measured at various scan rates of CV for another freshly prepared electrode potentiostatically polarized in 1 M $NaNO_3$ at 1.8 V (versus RHE) for 20 min are shown in Fig. 8b. Note that all CV curves in Fig. 8 were measured in 0.5 M H_2SO_4. Curve 1 in Fig. 8a show the typical voltammetric behavior of this ACF-pasted electrode in H_2SO_4; i.e., high background currents with a rise in currents with the positive shift of electrode potentials on both positive and negative sweeps in the investigated potential range. On curve 2, the above phenomenon becomes less obvious after the *potentiostatic polarization* in H_2SO_4 while a slight loss in voltammetric charges on both positive and negative sweeps is found. The former result indicates the better capacitive responses of this modified sample. On the other hand, the actual reasons responsible for the decrease in specific capacitance of ACF after *potentiostatic polarization* are still unclear although a too high density of the oxygen-containing functional

Table 1
Effects of electrochemical polarization modes, pretreated electrolytes, and test electrolytes on the specific capacitance of ACF-pasted electrodes deduced from the CV curves measured at 25 mV s^{-1}

Pretreatment of ACF	Test electrolytes		
	$NaNO_3$ (F g^{-1})	H_2SO_4 (F g^{-1})	Na_2SO_4 (F g^{-1})
As-prepared	76	87	55
Potentiodynamic polarization in $NaNO_3$	100	152	65
Potentiostatic polarization in $NaNO_3$	99	153	68
Potentiostatic polarization in H_2SO_4	35	89	25
Potentiostatic polarization in Na_2SO_4	40	125	38

groups may be attributed to this phenomenon [22], depressing the movement of solvated ions within the micropores. In Fig. 8b, relatively rectangular CV curves are obtained, indicating that the capacitive characteristics of ACF potentiostatically polarized in $NaNO_3$ are better than that of ACF potentiostatically polarized in H_2SO_4. In addition, voltammetric charges (see curve 1 in Fig. 8b) of the former sample are obviously higher than that of the latter, indicating the higher capacity of the former electrode. Based on the above results and discussion, *potentiostatic polarization* in $NaNO_3$ under a mild oxidation condition is a useful mode in promoting the specific capacitance of ACFs.

Table 1 shows the effects of electrochemical polarization modes, pretreated electrolytes, and test electrolytes on the specific capacitance of ACF-pasted electrodes deduced from the CV curves measured at 25 mV s^{-1}. Note that the sequence of test electrolytes with respect to decreasing the specific capacitance of unmodified and modified ACFs is: $H_2SO_4 > NaNO_3 > Na_2SO_4$. This result reveals that charges stored within the electric double layer are strongly affected by the moving rate of solvated ions within the micropores of ACF. The highest specific capacitance of ACF is obtained in H_2SO_4, attributable to the proton hopping mechanism since water molecules can act as a proton donor and acceptor [21]. On the other hand, due to the larger atom group and higher surface charge density of SO_4^{2-}, the electrochemical reversibility of ACF in this electrolyte is not as ideal as that in $NaNO_3$. From a comparison of the data shown in rows 3–5, the mild *potentiostatic polarization* in 1 M $NaNO_3$ has a positive effect on promoting the specific capacitance of ACF. However, the electrochemical modes used in this work possess insignificant effect on the specific capacitance. From a comparison of the data shown in last

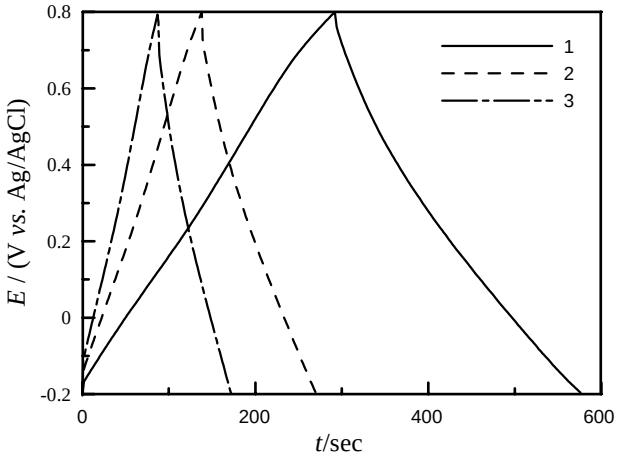

Fig. 9. Chronopotentiograms of an ACF-pasted electrode potentiostatically polarized at 1.8 V (vs. RHE) for 20 min in 1 M $NaNO_3$. CP curves were measured in 0.5 M H_2SO_4 solutions between −0.2 and 0.8 V at (1) 10 mA cm^{-2}; (2) 20 mA cm^{-2}; and (3) 30 mA cm^{-2}.

three rows, the specific capacitance of ACFs is strongly dependent on the electrolytes employed in the electrochemical pretreatments. In addition, the sequence of pretreated electrolytes with respect to decreasing the specific capacitance of these modified ACFs is: $NaNO_3 > Na_2SO_4 > H_2SO_4$. The above results may be due to a combination of two effects. First, the specific surface area of ACF is decreased when it has been subjected to *potentiostatic polarization* (see Table 2). Accordingly, double-layer capacitance should decrease with the *potentiostatic polarization* if there is no change in surface property for ACF after this pretreatment. Second, the density and structure of surface functional groups should be dependent upon the electrolytes and potentials employed. If the density of ionic functional groups is too heavy, the movement of ions with the same electric property should be depressed by the electrostatic interactions between the surface functional groups and ions. Based on the above results and discussion, the electrochemical pretreatment is expected to be not always good for promoting the specific capacitance of ACFs.

Typical chronopotentiograms of an ACF-pasted electrode, potentiostatically polarized in 1 M $NaNO_3$ at 1.8 V (versus RHE) for 20 min, measured in 0.5 M H_2SO_4 between −0.2 and 0.8 V at 10, 20 and 30 mA cm^{-2} are shown in Fig. 9 as curves 1–3, respectively. Note that the *i*R drop on all curves is more obvious than the three curves in Fig. 6, which is

Table 2
Physical properties of ACFs before and after potentiostatic polarization at 1.8 V (vs. RHE) for 20 min in various electrolytes

	ACF as-received	ACF polarization in $NaNO_3$	ACF polarization in H_2SO_4	ACF polarization in Na_2SO_4
Surface area (m^2 g^{-1})	862.7	724.6	746.0	695.3
Pore volume (cm^3 g^{-1})	0.4654	0.2779	0.2748	0.2671
Mesopore (%)	8	<1	<1	<1
Micropore (%)	92	>99	>99	>99
Mean pore size (Å)	29.2	18.7	14.3	13.7

significantly increased with increasing the applied current density. The above results indicate that the internal resistance of this ACF-pasted electrode should be increased by the electrochemical polarization in aqueous media. This effect is likely due to a slight damage of the graphite structure for the carbon fibers on the ACF by potentiostatic polarization. Fortunately, the charge curves are approximately linear and symmetric to their corresponding discharge curves. Hence, the specific capacitance of this modified ACF can be estimated by means of Eq. (1). Note that the specific capacitance of this ACF-pasted electrode measured at 10, 20, and 30 mA cm^{-2} is ca. 248, 229, and 217 F g^{-1}, respectively, which are very close to the value estimated from the CV curve measured at 10 mV s^{-1} (ca. 208 F g^{-1}). The average power density of this modified ACF measured at 10, 20, and 30 mA cm^{-2} is equal to ca. 0.43, 0.85, and 1.25 kW kg^{-1}, respectively. Based on the symmetric and similar *E–t* curves in Fig. 9 and the above power density data, this ACF-pasted electrode potentiostatically polarized in $NaNO_3$ shows the high-power characteristics with a much higher capacity, which is believed to be very suitable for the application of supercapacitors.

3.4. Textural characteristics of ACFs

The above difference in specific capacitance for ACFs with and without the electrochemical pretreatment may be due to the increase of specific surface area when ACF was polarized under a mild oxidation condition. Accordingly, the porous structures of this ACF before and after potentiostatic polarization at 1.8 V (versus RHE) for 20 min in 1 M $NaNO_3$, 0.5 M H_2SO_4 and 0.5 M Na_2SO_4 were analyzed in this work and their data were shown in Table 2. Note that most pores distributed within the as-prepared ACF are microporous (i.e., <2 nm). Accordingly, a large portion of inner surface area is not freely accessible for electrolytes to establish a complete electrical double-layer. Therefore, the specific capacitance of ACF is much smaller than that estimated from the specific surface areas of ACF (ca. 173 F g^{-1}). On the other hand, the potentiostatic polarization causes the completely loss of mesopores, resulting in the obvious decrease in mean pore size from 2.9 to ca. 1.9, 1.4 and 1.4 nm when $NaNO_3$, H_2SO_4 and Na_2SO_4 were respectively employed as the pretreated electrolyte. Moreover, the pore volume within these ACFs is significantly reduced after the above polarization. This phenomenon is attributable to the significant formation of oxygen-containing functional groups within the pores expelling the adsorption of nitrogen (see XPS results), which is supported by the significant decrease in specific surface area of ACF with potentiostatic polarization. Based on the above results and discussion, the obvious increase in specific capacitance for the ACF with the potentiostatic polarization in 1 M $NaNO_3$ at 1.8 V for 20 min is reasonably attributed to the increase in its ion adsorption and/or ion exchange abilities as well as the significant Faradaic pseudocapacitance.

From the above results and discussion, the higher capacity of ACF with potentiostatic polarization in $NaNO_3$ should be linked to the intrinsic structure (e.g., the distribution of neutral carbon (C–C or C=C), hydroquinone (–C–OH), quinone (–C=O), carbonyl group (O=C–OH), etc.) of oxygen-containing functional groups formed under a mild oxidation condition. These expectations can be quantitatively illustrated by examining the XPS core level spectra of C 1 s. Typical XPS core level spectra of C 1 s for the ACF-pasted electrode without and with the potentiostatic polarization in 1 M $NaNO_3$, 0.5 M H_2SO_4 and 0.5 M Na_2SO_4 are shown in Fig. 10a–d, respectively. Note that all core level spectra show relatively broad peaks, indicating the existence of several structures. Thus, the XPS peaks of C 1 s in Fig. 10a–d are reasonably decomposed into four Gaussian peaks with their binding energy respectively centered at 284.3, 286.3, 288.3 and 289.4 eV. The main C species on the ACF-pasted electrode is the neutral C atoms (i.e., peak centered at 284.3 eV). The peak centered at 286.3 is attributed to the C atoms with the C–OH single bond [23–25]. The highest binding energy is due to the presence of carbonyl carbons which are formed by the attack of water molecules during the potentiostatic polarization [25–27]. Thus, the relative area of these sub-peaks can be used to calculate the relatively density of oxygen-containing functional groups within the ACF. These results are shown in Table 3. From Table 3, the neutral C–C species were decreased from 73.7 to 69.9, 45.3, 43.0 at% when ACFs were potentiostatically polarized in 1.0 M $NaNO_3$, 0.5 M H_2SO_4 and 0.5 M Na_2SO_4, respectively. In addition, the C–OH species were enriched when SO_4^{2-} was used as the pretreated electrolyte. The former result reveals that the electrochemical pretreatment is a powerful tool for the formation of the oxygen-containing functional groups. In addition, the mean oxidation state of surface carbon species is obviously higher for the ACFs with potentiostatic polarization in SO_4^{2-} in comparison with that modified in $NaNO_3$. In fact, this mild oxidation favors the presence of C=O/C–OH and carbonyl groups. The former species should act as redox centers on the ACF-pasted electrode, providing the Faradaic pseudocapacitance (i.e., $C{=}O + H^+ + e = C{-}OH$). The carbonyl group should provide the active sites for the specific adsorption and/or exchange of cations. On the other hand, the latter result suggests that SO_4^{2-} favor the formation of

Table 3
The relative density of various oxygen-containing functional groups within ACFs before and after potentiostatic polarization at 1.8 V (vs. RHE) for 20 min in various electrolytes

ACF	Surface functional groups			
	C–C (%)	C–OH (%)	C=O (%)	O=C–OH (%)
As-received	73.7	19.8	5.1	1.4
Polarization in $NaNO_3$	69.9	18.5	8.3	3.3
Polarization in H_2SO_4	45.3	41.4	8.1	5.2
Polarization in Na_2SO_4	43.0	41.0	7.1	8.9

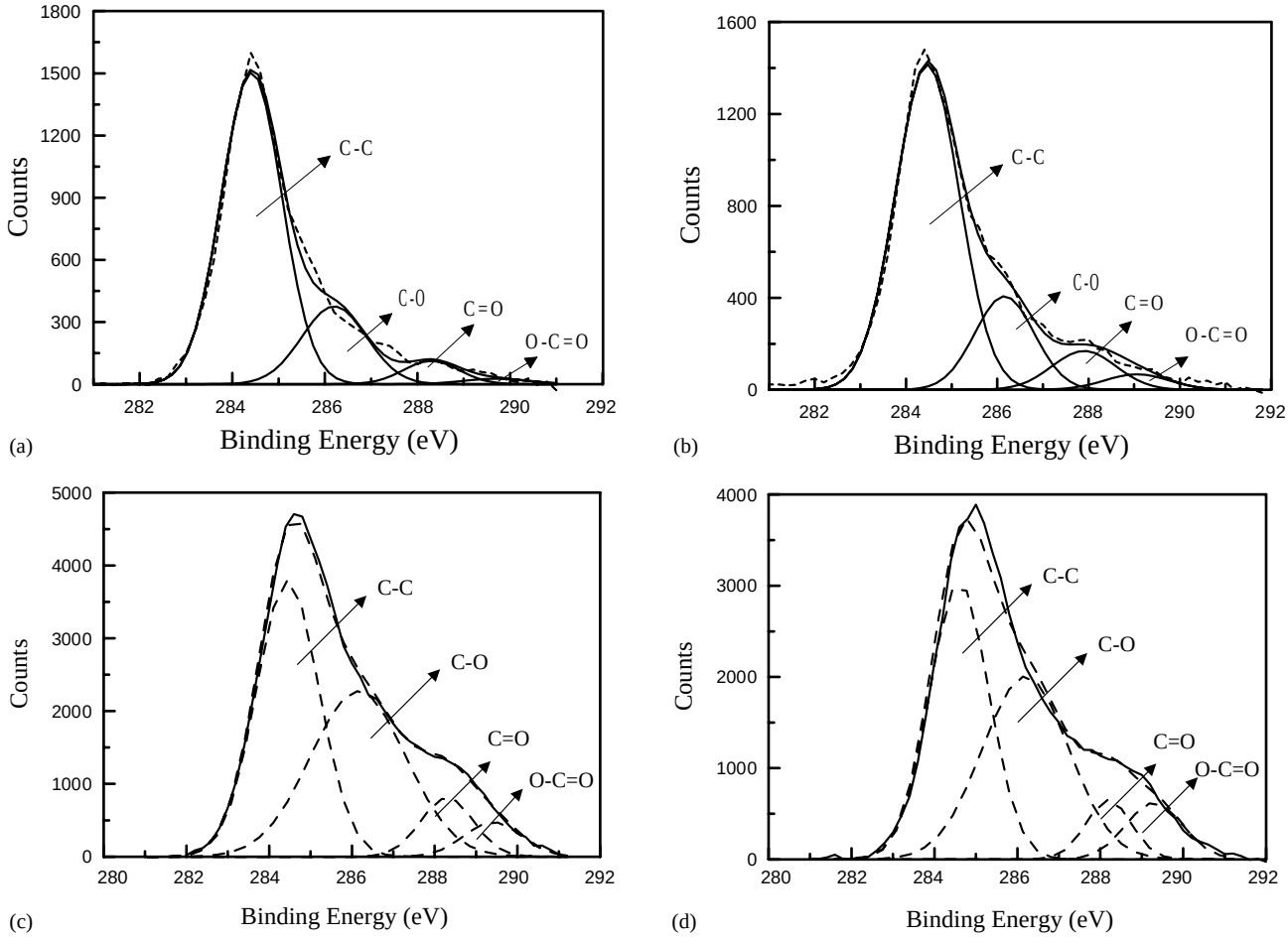

Fig. 10. X-ray photoelectron spectra of C 1 s for ACF (a) without and with potentiostatic polarization at 1.8 V (vs. RHE) for 20 min in (b) 1 M $NaNO_3$; (c) 0.5 M H_2SO_4 and (d) 0.5 M Na_2SO_4.

C–OH and the density of C–OH seems to be so heavy that the movement of ions within the micropores was significantly depressed by the surface functional groups. Based on all the above results and discussion, the highest specific capacitance of ACF with the potentiostatic polarization in $NaNO_3$ is reasonably attributed to the formation of a suitable density of oxygen-containing functional groups.

4. Conclusions

The ACF-pasted graphite electrode, modified with *potentiostatic polarization* at 1.8 V (versus RHE) in 1 M $NaNO_3$ for 20 min, with a high capacity and high-power charge–discharge characteristics between −0.2 and 0.8 V in 0.5 M H_2SO_4, was demonstrated to be a promising electrode material for supercapacitors. The average specific capacitance of this modified ACF estimated from the chronopotentiometric data could reach ca. 250 F g^{-1} between −0.2 and 0.8 V under a current density of 10 mA cm^{-2}. The voltammetric curves of ACF-pasted electrodes reached the ideal capacitive behavior when the PVDF content in the electronically conductive paste is 40 wt.%. The capacitive characteristics of ACF in $NaNO_3$ are better than that in H_2SO_4 and Na_2SO_4 although the specific capacitance of ACF-pasted electrodes measured in H_2SO_4 is much higher in comparison with the other two electrolytes. The increase in specific capacitance for the ACF-pasted electrode with *potentiostatic polarization* in $NaNO_3$ is attributed to the presence of a suitable density of oxygen-containing functional groups identified by means of X-ray photoelectron spectroscopy (XPS).

Acknowledgements

The financial support of this work, by the National Science Council of the Republic of China under contract no. NSC 91-2214-E-194-012, is gratefully acknowledged.

References

[1] B.E. Conway, Electrochemical Supercapacitors, Kluwer-Plenum Publishing Co., New York, 1999.
[2] A. Burke, J. Power Sources 91 (2000) 37.
[3] C.-C. Hu, K.-H. Chang, J. Power Sources 112 (2002) 401.

[4] Y.-R. Nian, H. Teng, J. Electrochem. Soc. 149 (2002) A1008.
[5] Y. Kibi, T. Saito, M. Kurata, J. Tabuchi, A. Ochi, J. Power Sources 60 (1996) 219.
[6] D. Qu, H. Shi, J. Power Sources 74 (1998) 99.
[7] C.-C. Hu, Y.-H. Huang, J. Electrochem. Soc. 146 (1999) 2465.
[8] C.-C. Hu, K.-H. Chang, Electrochim. Acta 45 (2000) 2685.
[9] C.-C. Hu, T.-W. Tsou, Electrochem. Comm. 4 (2002) 105.
[10] S. Shiraishi, H. Kurihara, H. Tsubota, A. Oya, Y. Soneda, Y. Yamada, Electrochem. Solid State Lett. 4 (2001) A5.
[11] C. Niu, E.K. Sichel, R. Hoch, D. Moy, H. Tennent, Appl. Phys. Lett. 70 (1997) 1480.
[12] E. Frackowiak, K. Jurewicz, S. Delpeux, F. Beguin, J. Power Sources 97–98 (2001) 822.
[13] D.T. Fagan, I. Hu, T. Kuwana, Anal. Chem. 57 (1985) 2759.
[14] R.J. Rice, N. Pontikos, R.L. McCreery, J. Am. Chem. Soc. 112 (1990) 4617.
[15] A. Ahmadpour, D.D. Do, Carbon 34 (1996) 471.
[16] R.C. Engstrom, V.A. Strasser, Anal. Chem. 56 (1984) 136.
[17] L.J. Krpley, A.J. Bard, Anal. Chem. 60 (1988) 1459.
[18] I. Hu, D.H. Karweik, T. Kuwana, J. Electroanal. Chem. 188 (1985) 59.
[19] S. Evans, W.S. Hamilton, J. Electrochem. Soc. 113 (1966) 1314.
[20] D.C.S. Tse, T. Kuwana, Anal. Chem. 50 (1978) 1315.
[21] A.J. Bard, L.R. Faulkner, Electrochemical Methods, Fundamentals and Applications, Wiley Sons, Singapore, 1980.
[22] P.T. Kissinger, W.R. Heineman, Laboratory Techniques in Electroanalytical Chemistry, second ed., Marcel Dekker, Hong Kong, 1996.
[23] J.G. Eaves, H.S. Munro, D. Parker, Polym. Commun. 28 (1987) 38.
[24] J.M. Ribo, A. Dicko, J.M. Tura, D. Bloor, Polymer 32 (1991) 728.
[25] C.D. Wagner, W.M. Riggs, L.E. Davis, J.F. Moulder, G.E. Muilenberg (Eds.), Handbook of X-ray Photoelectron Spectroscopy, Perkin-Elmer, Minnesota, 1979.
[26] F. Beck, Electrochem. Acta 33 (1988) 839.
[27] R. Erlandsson, O. Inganas, I. Lundstrom, W.R. Salaneck, Synth. Met. 10 (1985) 303.